SUPPLEMENTARY INFORMATION

METHODS

Synthesis of PLX4032

PLX4032 was synthesized from commercially available 5-bromo-7-azaindole and 2,4-difluoroaniline as described in WO2007002433. 5-Bromo-7-azaindole was reacted with 4(chlorophenyl)boronic acid under Suzuki coupling conditions to provide 5-(4-chloro-phenyl)-1H-pyrrolo[2,3-b]pyridine (**2).** Synthesis of propane-1-sulfonic acid (2,4-difluoro-3-formyl-phenyl)-amide (**3)** from 2,4-difluoroaniline was described elsewhere.[6] Compounds **2** and **3** under aldol reaction conditions provided a mixture of **4a** and **4b** which upon demethylation and oxidation provided N-[3-[5-(4-chlorophenyl)-1H-pyrrolo[2,3-b]pyridine-3-carbonyl]-2,4-difluoro-phenyl]propane-1-sulfonamide, **1 (PLX4032)**.

Scheme 1

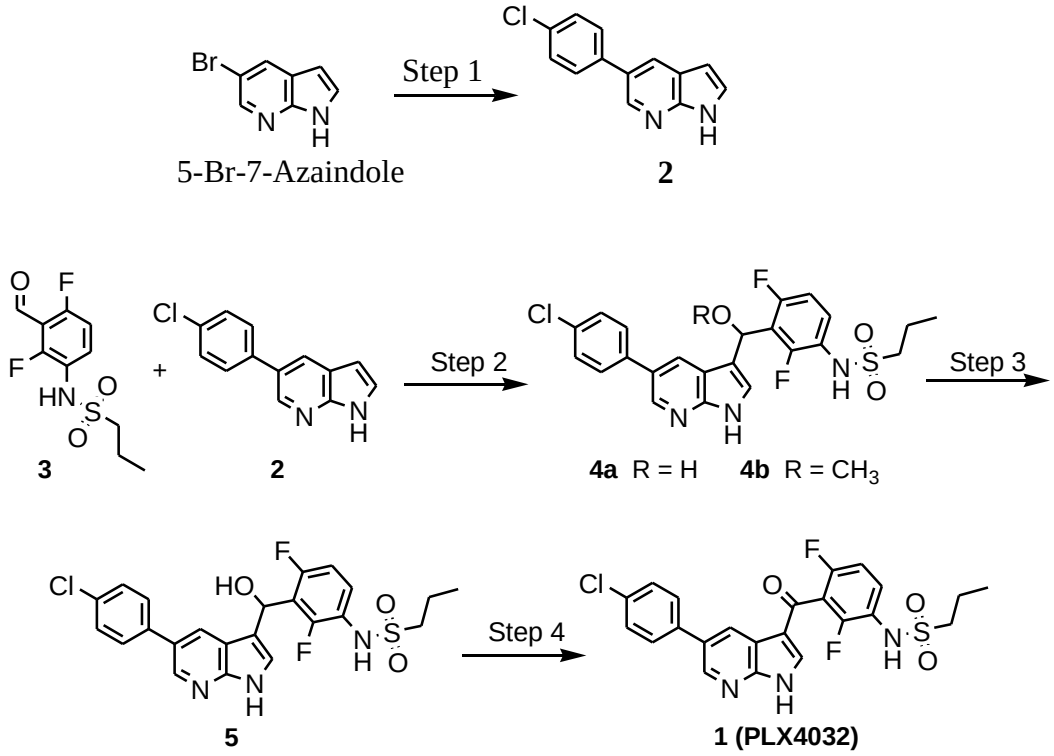

Step 1 – Preparation of 5-(4-chloro-phenyl)-1H-pyrrolo[2,3-b]pyridine (2). To 5-bromo-7-azaindole (70.6 g, 358 mmol) and 4(chlorophenyl)boronic acid (67.3 g, 430 mmol) in 700 mL of 1,2-dimethoxyethane was added a solution of potassium carbonate (59.4 g, 430 mol) in 350 mL of water. The resulting mixture was purged with nitrogen for 30 min and then

bis(triphenylphosphine)dichloropalladium(II) (25.3 g, 35.8 mmol) was added. The reaction mixture was heated at reflux overnight and the volatiles were removed under reduced pressure. The crude residue was taken up in 400 mL of brine and extracted with ethyl acetate (3 x 500 mL). The combined organic layers were dried over sodium sulfate, filtered, and the resulting filtrate was evaporated *in vacuo* to give a crude solid that was purified on a silica gel column (1.5 kg) with 1:4 to 1:1 ethyl acetate:heptane as eluent to provide 66.6 g (81%) of **2** as a tan solid. m.p.: 216-218 °C; ^{1}H-NMR (400 MHz, DMSO-d_6) δ 11.74 (s, 1H), 8.49 (s, 1H), 8.19 (s, 1H), 7.71 (d, J = 8.2 Hz, 2 H), 7.50 (s, 1H), 7.49 (d, J = 8.2 Hz, 2 H), 6.48 (m, 1H); ^{13}C-NMR (100 MHz, DMSO-d_6) δ 148.8, 142.1, 138.7, 132.4, 129.6, 129.3, 127.8, 127.5, 126.8, 120.3, 100.9; MS(ESI)[M+H^+] = 229.1.

Step 2 – Preparation of propane-1-sulfonic acid (3-{[5-(4-chloro-phenyl)-1H-pyrrolo[2,3-b]pyridin-3-yl]-hydroxy-methyl}-2,4-difluoro-phenyl)-amide (4a) and Propane-1-sulfonic acid (3-{[5-(4-chloro-phenyl)-1H-pyrrolo[2,3-b]pyridin-3-yl]-methoxy-methyl}-2,4-difluoro-phenyl)-amide (4b). To a suspension of 5-(4-chloro-phenyl)-1H-pyrrolo[2,3-b]pyridine (**2**, 64.9 g, 284 mmol) and propane-1-sulfonic acid (2,4-difluoro-3-formyl-phenyl)-amide (**3**, 90.4 g, 343 mmol) in methanol (1.8 L) in a water bath was added potassium hydroxide (129 g, 2.3 mol). The reaction was allowed to stir for 72 hours at room temperature and then adjusted to pH 7 with 4N hydrochloric acid (580 mL). The resulting mixture was evaporated *in vacuo* to remove methanol and extracted with ethyl acetate (3 x 800 mL). The combined organic layers were dried over sodium sulfate and evaporated *in vacuo* to give a crude oil. The crude oil was triturated with 3:1 MTBE/heptane (500 mL) to give a 1:3 solid mixture of **4a** and **4b** that was used directly for the next step. For compound **4b**: ^{1}H-NMR (400 MHz, DMSO-d_6) δ 11.79 (s, 1H), 9.60 (s, 1H), 8.49 (s, 1H), 8.06 (s, 1H), 7.66 (d, J = 8.59 Hz, 2H), 7.51 (d, J = 8.21, 2H), 7.37 (m, 1H), 7.32 (s, 1H), 7.11 (m, 1H), 6.06 (s, 1H), 3.35 (s, 3H), 2.96 (m, 2H), 1.63 (m, 2H), 0.84 (m, 3H); ^{19}F-NMR (376 MHz, DMSO-d_6) δ -116.15, -121.52; MS(ESI)[M+H^+] = 506.2.

Step 3 – Preparation of propane-1-sulfonic acid (3-{[5-(4-chloro-phenyl)-1H-pyrrolo[2,3-b]pyridin-3-yl]-hydroxy-methyl}-2,4-difluoro-phenyl)-amide (5). To a solution of **4a** and **4b** (~284 mmol) in acetic acid (750 mL) was added 48% (wt) aqueous solution of hydrobromic acid (150 mL). The resulting mixture was allowed to stir overnight at room temperature and then

evaporated *in vacuo*. The crude residue was dissolved in ethyl acetate (1 L) and water (1 L), and adjusted to pH 7 with solid potassium carbonate. The layers were separated and the aqueous layer was extracted with ethyl acetate (2 x 1 L). The combined organic layers were dried over sodium sulfate, filtered, and the resulting filtrate was evaporated *in vacuo* to give **5** as viscous oil that was used directly for the next step. ^{1}H-NMR (400 MHz, DMSO-d_6) δ 11.66 (s, 1H), 9.55 (s, 1H), 8.47 (s,1H), 7.97 (s, 1H), 7.62 (d, J = 8.59 Hz, 2H), 7.50 (d, J = 8.59 Hz, 2 H), 7.32 (m, 1H), 7.28 (m, 1H), 7.06 (m, 1H), 6.38 (d, J = 5.08, 1H), 6.08 (d, J = 5.08, 1H), 2.95 (m, 2H), 1.63 (m, 2H), 0.83 (m, 3H); ^{13}C-NMR (100 MHz, DMSO-d_6) δ 148.98, 142.24, 138.61, 132.53, 129.65, 129.18, 127.74, 127.31, 125.57, 124. 52, 122.22, 121.48, 118.38, 116.49, 112.52, 112.30, 60.99, 54.14, 17.48, 13.19; ^{19}F-NMR (376 MHz, DMSO-d_6) δ -116.49, -122.00; MS(ESI)[M+H^+] = 492.0.

Step 4 – Preparation of Propane-1-sulfonic acid {3-[5-(4-chloro-phenyl)-1H-pyrrolo[2,3-b]pyridine-3-carbonyl]-2,4-difluoro-phenyl}-amide, 1 (PLX4032) . To a solution of **5** in 1,4-dioxane (700 mL) was added 2,3-dichloro-5,6-dicyanobenzoquinone (83.8 g, 369 mmol) followed by water (35 mL). The resulting mixture was allowed to stir for 2 hours at room temperature and then treated with saturated aqueous sodium bicarbonate (700 mL). The mixture was evaporated *in vacuo* to remove 1,4-dioxane and extracted with ethyl acetate (3 x 1L). The combined organic layers were dried over sodium sulfate, filtered, and the resulting filtrate was evaporated *in vacuo* to give a crude solid that was purified on a silica-gel column (3 kg) with 95:5 dichloromethane:methanol as eluent to provide 78.7 g (45% for 3 steps) of **1 (PLX4032)** as a white solid. m.p.: 264 °C; ^{1}H-NMR (400 MHz, DMSO-d_6) δ 13.03 (s, 1H), 9.79 (s, 1H), 8.71 (s, 1H), 8.65 (br s, 1H), 8.25 (br s, 1H), 7.76 (d, J = 8.5 Hz, 2H), 7.60 (m, 1H), 7.52 (d, J = 8.4 Hz, 2H), 7.28 (m, 1H), 3.13 (m, 2H), 1.75 (m, 2 H), 0.95 (m, 3H); ^{13}C-NMR (100 MHz, DMSO-d_6) δ 180.6, 156.0, 152.3, 149.0, 143.9, 138.9, 137.0, 132.5, 130.3, 129.0, 128.9, 128.7, 127.1, 121.9, 118.1, 117.5, 115.7, 112.3, 53.5, 16.8, 12.6; ^{19}F-NMR (376 MHz, DMSO-d_6) δ -38.7, -44.1; IR (KBr) 3267, 3124, 1639, 1322, 1143 cm^{-1}; MS(ESI)[M+H^+] = 490.3; elemental analysis (% calcd, % found for $C_{23}H_{18}ClF_2N_3O_3S$): C (56.39, 56.18), H (3.70, 3.72), Cl (7.24, 7.52), N (8.58, 8.60), O (9.80, 9.80), F (7.76, 8.02), S (6.54, 6.57).

Preclinical studies. Expression and purification of B-RAF, structure determination, and protein kinase activity measurements were carried out as previously described.[6] To obtain co-crystals of B-RAF^{V600E} with PLX4032, the protein solution was initially mixed with the compound dissolved in DMSO at a final compound concentration of 1 mM. This complex was co-crystallized by a sitting drop vapor diffusion experiment in which equal volumes of complex (at 10 mg/ml concentration) and reservoir solution (100mM BisTris at pH 6.0, 12.5% 2,5-hexanediol, and 12% PEG3350) were mixed and allowed to equilibrate against the reservoir at 4°C. The crystal was soaked in cryosolvent, followed by flash-freezing in liquid nitrogen. The data were collected at Beamline ALS831 (Lawrence Berkeley National Laboratory, Berkeley, CA) with the wavelength of 1.11Å. The Ramachandran plot from the refined structure shows that 94%, 5.6% and 0.4% residues are in the most favored, additional allowed and generously allowed regions, respectively. A summary of the crystallography statistics is included in Supplementary Table 3. COLO205 tumor xenograft studies (Molecular Imaging Research, Ann Arbor, MI) were carried out as previously described either using a conventional formulation (5%DMSO, 1%methylcellulose)[6] or using the MBP formulation.[4]

Clinical methods have been recently described.[5]

Patient Population

All patients enrolled in the extension cohort of the Phase 1 study had provided melanoma tumor tissue for centralized confirmation of *BRAF* mutation status. Specimens were analyzed with an assay (investigational use only, Roche Molecular Systems, Inc., Pleasanton, CA) designed to specifically detect the *BRAF^{V600E}* (1799 T>A) mutation in DNA isolated from formalin-fixed, paraffin-embedded tumor tissue using previously described TaqMan® methodology.[8]

Histology and Immunohistochemistry of Tumor Biopsies

Semi-quantitative immunohistochemistry was performed on 5 μm-thick formalin-fixed paraffin-embedded tumor biopsies following H&E staining to determine pathologic diagnosis and tissue morphology and integrity. Antibodies to phosphorylated ERK (Cell Signaling Technology) and Ki67 (clone 30.9 rabbit mAb, Ventana or DakoCytomation, Carpinteria, CA) were used to immunostain the slides. IHC staining was visualized using iView DAB Detection kit (Ventana), the ultraView™ Universal DAB Detection Kit (Ventana) or the EnVision+ HRP DAB system

(DakoCytomation). Rabbit (DA1E) mAb IgG XP™ Isotype Control (Cell Signaling Technology, diluted 1:30.000 in Dako REAL Antibody Diluent) and CONFIRM Negative Control Rabbit Ig (Ventana) was substituted with the primary antibody as a negative control for pERK and Ki67 respectively. Alternatively, normal mouse serum (1:1000 dilution) was substituted for the primary antibody in each case as a negative control.

The degree of phospho-ERK staining in the nucleus and cytoplasm was interpreted semiquantitatively by assessing the intensity and extent of staining on the entire tissue sections present on the slides. The percent area of positively staining tumor cells was multiplied by their degree of staining (none [0], weakly [1], moderate [2], strong [3] staining cells). A staining score (H-score) was then calculated (out of a maximum of 300) equaling the sum of 1 x percentage of weak, 2 x percentage of moderate, and 3 x percentage of strong staining. The sum of these groups equated with the overall percentage of positivity (H-score). The repeatability and reproducibility of the phospho-ERK staining profile were assessed by comparing two runs for five tumor samples and three positions were assessed for each sample. The concordance was 100%. Bland- Altman analysis of the H-scores of the cytoplasmic and nuclear staining compartments confirmed excellent reproducibility.[29] For Ki67 staining, the percentage of positive cells was determined. At the University of Pennsylvania, all slides from patients 12-48 were reviewed by a single dermatopathologist (X.X.). All slides from paired biopsies from patients 56-93 were evaluated at HistoGeneX (Belgium) by L Andries (Ki67) and M Knaapen (pERK). In order to make sure that there was consistency in readings across pathologists, five paired (pre- and post-treatment) stained slides for Ki67 and phospho-ERK (nuclear, cytoplasm) were provided in a blinded fashion from the University of Pennsylvania to HistoGeneX and vice versa.

RESULTS

PLX4032 kinase selectivity

As mentioned in the text, when the kinase selectivity panel was expanded to over 200 members, several additional kinases were found to be sensitive to PLX4032. Most of these kinases were assayed at a lower ATP concentration (10 μM for the counter-screens versus 100 μM for the RAF kinases); since PLX4032 is a competitive inhibitor assay at the lower ATP concentration results in lower IC_{50} values. In a panel of over 150 chemical analogs of PLX4032, there was good correlation between biochemical potency for B-RAF^{V600E} and cellular activity against B-RAF-mutant cells. This correlation did not depend on the relative potency against B-RAF^{V600E} and wild type B-RAF. Therefore, we believe that efficacy in melanoma primarily derives from inhibition of mutant B-RAF; future studies may explore the role of off-targets in other indications.

PLX4032 structure

When PLX4032 was co-crystallized with B-RAF^{V600E}, two unique molecules of the kinase domain in the asymmetric unit adopt a side- to-side dimer configuration as observed in previous RAF crystal structures.[6,23,30] Previously, PLX4720 was co-crystallized with wild type B-RAF, and the protomer with only partial ligand occupancy (apo) adopts a DFG-out conformation representing the inactive state of the kinase. However, the apo-protomer in the PLX4032 co-structure with B-RAF^{V600E} displays the DFG-in conformation with the activation loop locked away from the ATP-binding site by a salt-bridge between Glu^{600} and Lys^{507} (Figure 1D). Subsequent analysis of the structure of PLX4720 co-crystallized with B-RAF^{V600E} revealed that the apo-protomer displays the DFG-in conformation, suggesting that this property is determined by the mutation. It is interesting to speculate that the conformation of the apo-protomer may determine the paradoxical activation described in the main text. The conformational difference captured by the crystal structures (Figure 1C) suggests that, although wild-type B-RAF is in a dynamic equilibrium between the active (DFG-in) and inactive (DFG-out) configurations, oncogenic BRAF mutations such as V600E induce constitutive kinase activity by shifting the equilibrium toward the active (DFG-in) configuration. We believe that selective binding to the DFG-in conformation may contribute to a wide safety margin because such inhibitors would

suppress the tumor growth but spare the important biological functions mediated by wild-type B-RAF kinases.

Clinical pharmacokinetics and efficacy

At the 960 mg BID dose, the steady state PLX4032 concentration of 86 ± 32 μM (mean ± SD) and the AUC $_{0\text{-}24}$ of 1741 ± 639 μM·h (mean ± SD are relatively high plasma drug concentrations.[5] For example, the efficacious AUC $_{0\text{-}24}$ values for the marketed kinase inhibitors imatinib and erlotinib are 81.2 μM·h and 67.4 μM·h, and the steady state concentrations are 2.5 μM and 3.0 μM, respectively.[31] Since the cellular potencies of PLX4032 are comparable to those of imatinib and erlotinib, the requirement for a high PLX4032 exposure derives from the very high plasma protein binding property: > 99.5% of the drug is bound to plasma protein, so the free drug fraction is low. By contrast, the plasma protein binding values for imatinib and erlotinib are ~95% and ~93%, respectively.[31]. The pharmacokinetic profile is also influence by the very low aqueous solubility of PLX4032.

Some degree of tumor regression (including four patients whose regressions did not qualify as PRs) could be measured in 30 of the 32 patients at the 960 mg BID dose, and 17 of the 32 patients had at least 50% reduction in tumor dimensions (30% being sufficient to qualify as PR by RECIST criteria). Interestingly, the only two patients who did not have measurable tumor regression at their first CT scan no longer required narcotics for pain shortly after beginning PLX4032 treatment; one of these patients who had been hypoxemic at baseline no longer required supplementary oxygen within the first week of dosing. These data suggest that all 32 patients in this cohort derived some benefit from B-RAF inhibition.

29. Bland, J.M. & Altman, D.G. Statistical methods for assessing agreement between two methods of clinical measurement. *Lancet* **1**, 307-310 (1986).
30. Wan, P.T., *et al.* Mechanism of activation of the RAF-ERK signaling pathway by oncogenic mutations of B-RAF. *Cell* **116**, 855-867 (2004).
31. van Erp, N.P., Gelderblom, H. & Guchelaar, H.J. Clinical pharmacokinetics of tyrosine kinase inhibitors. *Cancer Treat Rev* **35**, 692-706 (2009).

Supplementary Table 1. Biochemical IC_{50} determinations of the kinase inhibitory activity of PLX4032 versus a panel of kinases

Assay	IC_{50} nM*
B-RAF-V600E	31
C-RAF	48
B-RAF	100
SRMS	18
ACK1	19
MAP4K5 (KHS1)	51
FGR	63
LCK	183
BRK	213
NEK11	317
BLK	547
LYNB	599
YES1	604
WNK3	877
MNK2	1717
FRK (PTK5)	1884
CSK	2339
SRC	2389

*A list of over 200 kinases minimally affected by PLX4032 is included below.
Note that all RAF enzymes and SRMS were assayed at an ATP concentration of 100 μM, while all other kinases in the table above were assayed at an ATP concentration of 10 μM.

Kinases with <20% Inhibition at 1 μM:
ABL1, ABL2, ADRBK1, AMPK_A2, ARK5, Aurora_A-C, BMX, CDC42_BPA, CAMK2A, CDK5_p35, CSF1R, DYRK1B, EPHA5, EPHA8, EPHB4, FES, FLT3, FYN, GSK3beta, JAK1, KDR, KIT, MAP4K2, MAPK3, MARK2, MARK4, MATK, MET, MINK1, NEK1, NEK2, PAK3, PAK6, PDGFRbeta, PHKG1, PKBalpha, PKC_beta_I, PKC_beta_II, PKC_delta, PKC_gamma, PKC_zeta, SRC, STK4, STK24

Kinases with <10% Inhibition at 1 μM:
ACVR1B_(ALK4), ADRBK2_(GRK3), ALK, AMPK_A1/B1/G1, ASK1, AXL, BRSK1_(SAD1), BrSK2, BTK, CAMK1, CAMK1D, CAMK2B, CAMK2D, CaMKIdelta, CaMKIIbeta, CaMKIIdelta, CaMKIIgamma,,CDC42_BPB, CDK1/CyclinB, CDK2/CyclinA, CDK2/cyclinE, CDK3/cyclinE, CDK5_p25, CDK6/cyclinD3, CDK7/CyclinH/MNAT1,CDK9/CyclinT1, CHEK1, CHEK2, CK1delta, CK1gamma1, CK1gamma2, CK1gamma3, CK2alpha2, CLK1, CLK2, CLK3, CSNK1A1, CSNK1D, CSNK1E, CSNK1G1, CSNK1G2, CSNK1G3, CSNK2A1, CSNK2A2, DAPK1, DAPK2, DAPK3_(ZIPK), DCAMKL2_(DCK2), DDR2, DMPK, DRAK1, DYRK1A, DYRK2, DYRK3, DYRK4, EEF2K, EGFR, EPHA1, EPHA2, EPHA3 EPHA4, EPHA7, EPHB1, EPHB2, EPHB3, ERBB2, ERBB4, FER, FGFR1, FGFR2, FGFR3, FGFR4, FLT1, FLT4, FRAP1, GCK, GRK4, GRK5, GRK6, GRK7, GSK3A, HCK, HIPK, HIPK2, HIPK3, HIPK4, IGF1R, IGF-1R, IKBKB, IKBKE, IKKalpha, IKKbeta, INSR, INSRR, IRAK1, IRAK4, ITK, JAK2, JAK2_JH1_JH2, JAK3, JNK1alpha1, JNK2alpha2, LCK, LIMK1, LKB1, LOK, LTK, MAP2K1, MAP2K2, MAP2K6, MAP3K8, MAP3K9, MAP4K4, MAPK1, MAPK10, MAPK11, MAPK12, MAPK13, MAPK14, MAPK2, MAPK8, MAPK9, MAPKAPK2, MAPKAPK3, MAPKAPK5, MARK1, MARK3, MELK, MERTK, MKK7beta, MLCK, MRCKalpha, MRCKbeta, MST1R, MST4, mTOR/FKBP12, MUSK, NEK3, NEK4, NEK6, NEK7, NEK9, NLK, NTRK1, NTRK2, NTRK3, PAK2, PAK4, PAK7_(KIAA1264), PAR-1Balpha, PASK, PDGFRalpha, PDK1, PHKG2, PIK3CA/PIK3R1, PIK3CG, PIM1, PIM2, PIM-3, PKBbeta, PKBgamma, PKCalpha, PKCepsilon, PKCeta, PKCiota, PKCmu, PKCtheta, PKG1alpha, PKG1beta, PKN1, PLK2, PLK3, PRK2, PRKACA, PRKCA, PRKCE, PRKCH, PRKCI, PRKCN, PRKCQ, PRKD1, PRKD2, PRKG1, PRKG2, PRKX, PTK2, PTK2B, RET, RIPK2, ROCK1, ROCK2, ROS1, RPS6KA1, RPS6KA2, RPS6KA3, RPS6KA4, RPS6KA5, RPS6KA6, RPS6KB1, SGK, SGK2, SGKL, SIK, SNF1LK2, SNK, SRPK1, SRPK2, STK3, STK22B, STK22D, STK23, STK25, STK33, SYK, TAK1, TAO3, TAOK2, TBK1, TEC, TEK, TLK2, TXK, TYK2, TYRO3, ULK2, ULK3, VRK2, WNK2, WNK3, ZAP70

Supplementary Table 2. Semi-quantitative immunohistochemistry data

Patient #*	Daily Dose	Biopsy	AUC (µM·h)	pERK H-score *nucleus*	pERK H-score *cytoplasm*	Ki67	Patient tumor best response**
12	800	Pre Post	- 165	100 40	10 10	30% 5%	+ 3%
19	800	Pre Post	- 54	50 10	20 20	20% 5%	+ 32%
21	1600	Pre Post	- 118	60 11	10 10	60% 20%	+ 47%
26	1600	Pre Post	- 168	0 18	105 120	60% 25%	+ 29%
42	1440	Pre Post	- 1101	70 2	50 1	30% 5%	- 54%
44	640	Pre Post	- 399	100 2	70 2	50% 2%	Not assessable
45	640	Pre Post	- 662	NA 0.5	NA 70	NA 9%	- 70%
48	640	Pre Post	- 791	10 0	160 60	30% 1%	- 14%
56	1440	Pre Post	- 1079	12 9	70 2	NA NA	- 59%
60	1920	Pre Post	- 1859	125 0	120 15	18% 10%	- 21%
62	1920	Pre Post	- 2918	90 5	190 30	18% 3%	- 79%
65	1920	Pre Post	- NA	70 3	220 20	22% 20%	- 86%
76	1920	Pre Post	- 2552	165 10	260 20	40% 2%	- 100%
79	1920	Pre Post	- NA	155 30	205 45	64% 2%	- 60%
81	1920	Pre Post	- 1241	28 1	145 3	10% 1%	- 73%
85	1920	Pre Post	- 2717	240 0	290 117	53% 20%	- 23%
93	1920	Pre	- NA	27 0	126 5	7% 3%	- 50%

*Tumor biopsies from patients 12-48 were assessed at the University of Pennsylvania; assessment of the remaining biopsies was organized by Roche.

** Maximum percent reduction from baseline measurement of tumor dimensions; reductions of 30% or greater qualify as PRs by RECIST criteria.

Note that tumors of all patients in this table had $BRAF^{V600E}$ mutations.

NA, not available

Supplementary Table 3. Data collection and refinement statistics[§]

	PLX4032 in B-RAF^{V600E}
[§]**Data collection**	
Space group	$P2_12_12_1$
Cell dimensions	
a, *b*, *c* (Å)	50.8, 104.4, 110.1
α, β, γ (°)	90.0, 90.0, 90.0
Resolution (Å)	21.3-2.45 (2.58-2.45)*
R_{sym} or R_{merge}	7.2% (52.4%)
$I/\sigma I$	8.8 (1.4)
Completeness (%)	99.8 (99.8)
Redundancy	4.5(4.5)
Refinement	
Resolution (Å)	21.3-2.45
No. reflections	21,223
$R_{work/}$ R_{free}	21.3/25.8
No. atoms	
Protein	4002
Ligand/ion	33
Water	65
B-factors	
Protein	65.7
Ligand/ion	43.4
Water	44.1
R.m.s deviations	
Bond lengths (Å)	0.003
Bond angles (°)	0.7

Each asymmetric unit contains two BRAF^{V600E} molecules.
§ These data were collected from a single crystal.
* Highest resolution shell is shown in parenthesis.